Intrinsic compressive stress in polycrystalline films with negligible grain boundary diffusion

Brian W. Sheldon[a)]
Division of Engineering, Brown University, Providence, Rhode Island 02912

Adi Ditkowski
Division of Applied Mathematics, Brown University, Providence, Rhode Island 02912

R. Beresford, Eric Chason, and Janet Rankin
Division of Engineering, Brown University, Providence, Rhode Island 02912

(Received 14 November 2002; accepted 27 March 2003)

The model developed here describes compressive stress evolution during the growth of continuous, polycrystalline films (i.e., beyond the point where individual islands have coalesced into a continuous film). These stresses are attributed to the insertion of excess adatoms at grain boundaries. Steady state occurs when the strain energy at the top of the film is balanced by the local excess chemical potential of surface adatmos. Strain gradients associated with this compressive stress mechanism depend on the kinetics of the process. In the absence of grain boundary diffusion, these strain profiles are determined by the ratio of the atom insertion and growth rates. The steady-state strain and the strain evolution kinetics also depend on the two key length scales, the grain size, and the film thickness. The ratio of these two lengths (i.e., the grain aspect ratio) can also have a significant influence on the thermodynamic driving force for strain evolution if the grain sizes are sufficiently small. The model is fit to existing data for the growth of AlN films. However, more detailed comparisons will require experiments that are specifically designed to test this model.
 [DOI: 10.1063/1.1575916]

I. INTRODUCTION

Intrinsic compressive stresses occur during the deposition of many different polycrystalline films.[1–7] The Volmer–Weber growth mode proceeds by the initial formation of individual islands, followed by their coalescence into a continuous film. Compressive stresses prior to coalescence have been attributed to the Laplace pressure associated with surface energy effects.[8] The subsequent tensile stresses observed during and after island coalescence are usually attributed to grain boundary formation[2,6,9–12] or to grain growth.[13,14] The compressive stresses that occur after the formation of a continuous film are currently the subject of more uncertainty, and are the subject of this article.

We recently proposed that intrinsic compressive stresses in continuous polycrystalline films are driven by the excess chemical potential of surface adatoms produced by the growth flux.[15] In theory, this driving force could create intrinsic stress by incorporating additional atoms into the bulk growth surface, away from the grain boundaries (i.e., as interstitials or by creating additional lattice sites at dislocations). However, atom insertion at grain boundaries is expected to have a lower activation barrier than the formation of these other defects. This is consistent with experiments showing that the intrinsic compressive stresses observed in polycrystalline Pd films are not present in monocrystalline Pd deposited under the same conditions.[16] The previous steady-state formulation of Chason *et al.* assumes that grain boundary diffusion is fast, and that the extra atoms associated with compressive strain are incorporated at a constant rate.[15] The primary difference between this description and the model developed in Secs. II and III is that grain boundary diffusion is now assumed to be negligible (note that the adatom supersaturation provides the principle thermodynamic driving force for stress generation in both models). The model in the current article also develops a more complete kinetic description of time-dependent stress evolution (rather than just steady state) and we also consider modifications to the thermodynamic driving force based on grain size effects due to weighted mean curvature.

A key advantage of studying systems where grain boundary diffusion can be ignored is that detailed comparisons with experiments are accomplished more readily because the grain boundary diffusion kinetics do not have to be deconvoluted from the data. To demonstrate this, the model developed here is compared with existing data on AlN films. In comparing the model with other work, note that significant compressive stresses have generally been associated with high surface mobilities during film growth.[1,3,5] The model developed in Secs. II and III does not consider the surface mobility directly. Instead, it describes the evolution of intrinsic compressive stress by considering the competition between atom insertion at grain boundaries and the film growth rate. Possible connections between stress and the surface mobility are discussed briefly in Sec. IV.

II. MODEL FORMULATION

A. Thermodynamic considerations

The model is based on the film geometry in Fig. 1. Both islands and substrate are idealized as linear elastic solids with infinite out-of-plane thickness, such that deformation

a)Electronic mail: brian_sheldon@brown.edu

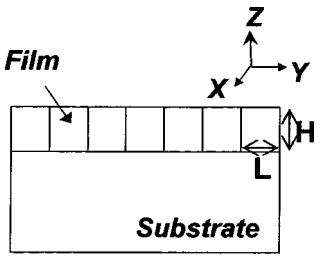

FIG. 1. Schematic of the film geometry.

occurs in plane strain. This conception is the basis for a relatively simple model that focuses on the kinetic competition between the growth rate and the incorporation of excess atoms at grain boundaries. The two key length scales are the grain size, L, and the film thickness, H (the substrate is assumed to be much thicker than the film). With the planar geometry in Fig. 1, the in-plane strain is treated as a constant average value, such that the strain varies only with vertical position, Z.

The chemical potential of the growth surface is given by

$$\mu_s = \mu^O + \frac{\gamma_b \Omega}{L} + \delta\mu_G , \tag{1}$$

where μ^O is the chemical potential of an atom in the bulk, Ω is the atomic volume, and γ_b is the grain boundary free energy. The final term in Eq. (1) is the excess chemical potential of surface adatoms due to the growth flux, which depends on the relative rates of various processes that occur on the growth surface. The excess chemical potential of the vapor, $\mu^{\mathrm{VAPOR}} - \mu^O$, is an upper bound on $\delta\mu_G$. If the attachment rate at atomic steps is fast relative to other surface processes, then the value of $\delta\mu_G$ near these steps will be much smaller than the vapor supersaturation (i.e., $\delta\mu_G$ can approach zero in some cases). For the purposes of our current analysis, surface processes are not considered in any detail, and the value of $\delta\mu_G$ is assumed to be constant during growth, with a value $0 < \delta\mu_G < (\mu^{\mathrm{VAPOR}} - \mu^O)$. Possible relationships between $\delta\mu_G$ and surface mobility are discussed briefly in Sec. IV.

The form of Eq. (1) follows our recent work,[15] except that the second term on the right-hand side of Eq. (1) has been added to account for interfacial energy effects associated with small grains. With the faceted grains in Fig. 1, these effects are described by the weighted-mean curvature (wmc), a concept pioneered by Taylor.[17] To understand the wmc in two dimensions, it is instructive to first consider isolated particles with fourfold symmetry, where the only energetically allowable surfaces are $\langle 01 \rangle$ facets with equal surface free energies. In this illustrative example there is no strain and the conventional Wulff construction describes an equilibrium shape which is a square, such that there is a thermodynamic driving force to move nonsquare grains towards their equilibrium shape. Applying this concept to the constrained film in Fig. 1 means that the relative surface and interface free energies will define an equilibrium aspect ratio for the grains. The general microstructure created by film growth will not adopt this aspect ratio (except possibly for one particular point in time during the growth process). Thus, the actual grain aspect ratio at any particular point has a wmc driving force that acts to move the grains toward their equilibrium shape. In the absence of grain growth, this wmc driving force should move material into the grain boundaries if H/L exceeds the equilibrium aspect ratio, and vice versa if the H/L value is less than the equilibrium aspect ratio.

The chemical potential of an atom along the grain boundary is given by

$$\mu_B = \mu^O + \frac{\Omega(\gamma_s + \gamma_I)}{H} - \Omega\sigma, \tag{2}$$

where the second term is again a wmc contribution, and γ_s and γ_I are the energy of the top facet and the substrate/film interface, respectively. The final term in Eq. (2) describes the contribution from stress in the film, where σ is the stress due to excess atoms incorporated into the film (i.e., relative to an unstressed crystal).

The driving force for inserting atoms into the grain boundary, $\Delta\mu$, is obtained by taking the difference between Eqs. (1) and (2) to give

$$\Delta\mu = \delta\mu_G + \Omega\left(\frac{\gamma_b}{\mathbf{L}} - \frac{(\gamma_S + \gamma_I)}{\mathbf{H}} + \sigma(\mathbf{H})\right), \tag{3}$$

where $\sigma(H)$ is the stress at the top of the grain boundary. The net wmc contribution in Eq. (3) accounts for the difference between the actual and equilibrium aspect ratio of the grains (i.e., the net wmc contribution is zero when the grains exhibit their equilibrium aspect ratio). Adding or removing atoms from the grain boundary may alter γ_b, and hence $\Delta\mu$, however, the average contributions from these variations are assumed to be negligible for the current treatment.

B. Film growth and adatom incorporation at grain boundaries

The model constructed here assumes that the growth process can add atoms to the film in two ways. Most material is added on the top surface by traditional crystal growth mechanisms, where each layer of atoms is templated onto the underlying crystalline lattice. This causes the new layer to mimic the stress state of the previous layer, as long as there are no relaxation mechanisms operating (e.g., dislocation formation, etc.).

The second mechanism is the introduction of excess atoms at the grain boundaries, driven by $\Delta\mu$ in Eq. (3). A net positive flux of atoms into the grain boundary will increase the in-plane compressive strain of the top layer. It is assumed that the average strain of the top layer of atoms can be divided into two components, with $\epsilon^{\mathrm{Surface}} = \epsilon^{\mathrm{Intrinsic}} + \epsilon$. The term $\epsilon^{\mathrm{Intrinsic}}$ accounts for the surface structure (i.e., the inherent surface tension). The value of ϵ is associated with phenomena which cause the number of atoms in the top layer to deviate from N_o, the number of atoms in an atomic layer of an unstressed bulk crystal. For the present analysis, we assume that $\epsilon^{\mathrm{Intrinsic}}$ is isotropic and independent of ϵ, and that surface stress effects do not cause any significant alterations in the surface free energy in the wmc terms in Eq. (3). In cases where these assumptions are not valid, the treatment employed here must be extended.

The number of extra atoms in a layer, N_E, is directly proportional to the strain:

$$\epsilon = -\frac{N_E}{N_O} = -\frac{\Omega N_E}{aBL}, \tag{4}$$

where a is the height of an unstrained layer, B is the grain boundary length in the x direction, and L is the grain size (see Fig. 1). The net flow of atoms into the grain boundary can be described by the following rate equation:

$$\frac{dN_E}{dt} = 2aB\Gamma_c[C_a - C_a^B], \tag{5}$$

where Γ_c is the jump rate for inserting atoms at the top of the boundary, C_a is the average concentration of adatoms on the growth surface (adjacent to the boundary), and C_a^B is the value of C_a in equilibrium with the top of the boundary (if the growth surface equilibrates with the top of the grain boundary, then $C_a = C_a^B$ and there is no net flux of atoms in the boundary). The factor of 2 in Eq. (5) appears because atoms can be inserted from both sides of the boundary.

In the kinetic formulation in Eq. (5), the chemical potential driving force in Eq.(3) is expressed as $C_a - C_a^B$ (i.e., the difference between the actual and equilibrium adatom concentrations at the boundary). To evaluate this directly, consider the relatively simple case where C_a is described by solution thermodynamics according to: $\mu_S = \mu^O + kT \ln[C_a/C^o]$, where C^o is the adatom concentration in equilibrium with an unstrained single crystal surface (which is also in equilibrium with the surrounding atmosphere when there is no growth flux). Combining this relationship between μ_S and C_a with Eq. (1) gives

$$C_a = C^o \exp\left[\frac{1}{kT}\left(\frac{\Omega\gamma_b}{L} + \delta\mu_G\right)\right]. \tag{6}$$

Using the same approach to evaluate C_a^B with Eq. (2) gives

$$C_a^B = C^o \exp\left[\frac{1}{kT}\left(\frac{\Omega(\gamma_S + \gamma_I)}{H} - \Omega\sigma_H\right)\right], \tag{7}$$

where σ_H, the stress at $Z = H$, is equal to $M\epsilon_H$. The plane strain film modulus is $M = E/(1-v^2)$, where E is Young's modulus and v is Poisson's ratio.

Combining Eqs. (4)–(7) then gives

$$\frac{d\epsilon}{dt} = -\frac{2\Omega}{L}\Gamma_c C^o\left(s_s - \exp\left[\frac{\Omega(\gamma_S + \gamma_I)}{H(kT)} - \frac{\Omega M\epsilon_H}{kT}\right]\right), \tag{8}$$

$$s_s = \exp\left[\frac{1}{kT}\left(\delta\mu_G + \frac{\gamma_b\Omega}{L}\right)\right] = s_s^o \exp\left[\frac{\psi_b}{\lambda}\right], \tag{9}$$

where $\psi_b = \Omega\gamma_b/a(kT)$. The surface supersaturation ratio, $s_s = C_a/C^o$, reflects the excess chemical potential at the growth surface, $\mu_S - \mu^O$. The value of $s_s^o = \exp(\delta\mu_G/kT)$ is the surface supersaturation due to only the growth flux. With the simplified grain structure in Fig. 1 (i.e., constant L), the wmc contribution in Eq. (9) is fixed and s_s is constant for a given set of growth conditions. In real films, L often increases as the film thickness increases. However, a constant value of L also approximates a columnar microstructure where the value of L changes very slowly.

The derivation leading to Eq. (8) is similar to the plane strain calculations that have been used elsewhere to evaluate intrinsic stress mechanisms.[11,12] Most experiments with thin films measure biaxial stress, which corresponds more closely to a square lattice of $L \times L$ square grains. This plane stress case can also be described by Eq. (8), by modifying the wmc terms to account for three-dimensional grains and by taking M as the biaxial modulus, $E/(1-v)$.

III. RESULTS

A. Strain profiles

The proposed mechanism for compressive strain evolution is described by Eq. (8). This formulation is applicable to a variety of different materials. Thus, the results in Secs. III A and III B are presented with general values for the key parameters, rather than choosing values for specific materials. A more specific discussion of data for AlN is presented in Sec. III C. It is also important to note that the excess chemical potential on the growth surface [i.e., $\delta\mu_G$ in Eq. (1)] is not always independent of L, primarily because of the potentially complex interactions between the kinetic processes occurring on the growth surface. In light of this complexity, $\delta\mu_G$ is treated as a constant that is independent of L for the calculated results that are presented here.

It is convenient to replace the time with the film thickness by dividing both sides of Eq. (8) by a constant growth rate, u, to get

$$\frac{d\epsilon}{dn} = -\frac{2a\Omega\Gamma_c C^o}{Lu}\left(s_s - \exp\left[\frac{\Omega\gamma_s}{an(kT)} - \frac{\Omega M\epsilon}{kT}\right]\right), \tag{10}$$

where $n = H/a$ is the film thickness in atom layers. Since our treatment assumes that grain boundary diffusion is absent, the strain in each layer is effectively locked in because atoms cannot move in response to the chemical potential gradient associated with the strain gradient through the film. Thus, Eq. (10) describes the strain profile that is created by the insertion mechanism described in Sec. II.

The initial condition for Eq. (10) depends on stresses that occur prior to and during the coalescence of isolated grains to produce a continuous film. With this in mind, a relatively simple initial condition of $\epsilon = \epsilon_o$ at $n = n_o$ was used to solve Eq. (10). This gives

$$\epsilon = \frac{1}{\beta}\ln\left[e^{\beta\epsilon_0} + \frac{2\beta\omega_c}{\lambda s_s}\int_0^{\Delta n}\exp\left(\frac{\psi_s}{\xi + n_o} + \frac{2\beta\omega_c}{\lambda}\xi\right)d\xi\right] - \frac{2\omega_c}{\lambda}\Delta n \tag{11}$$

where $\omega_c = \Gamma_c C^o s_s \Omega/u$, $\Delta n = n - n_o$, $\lambda = L/a$, $\beta = \Omega M/kT$, and $\psi_s = \Omega\gamma_s/a(kT)$. According to Eq. (11), the strain increases as the film grows, until it eventually approaches a steady-state limiting value given by

$$\epsilon_{ss} = -\frac{\ln(s_s)}{\beta}. \tag{12}$$

At ϵ_{ss} the rate at which atoms are inserted at the boundary is exactly equal to the rate at which excess boundary atoms can

move back to the surface. This means that there is no net change in stress as deposition proceeds beyond this point.

Physically, $2\omega_c/\lambda$ in Eq. (11) ratios the number of extra atoms inserted at the grain boundary to the number of atoms that are added to the growth surface, under conditions where $\epsilon=0$ and there are no wmc contributions. The definition of ω_c can be simplified by noting that $u=\Gamma_g C^o s_s \Omega/\eta_s$, where Γ_g is the jump frequency for incorporating an adatom at a step, and η_s is the average number of atomic spacings between steps (i.e., the average distance between steps is equal to $\eta_s a$). This leads to

$$\omega_c=\frac{\Gamma_c \eta_s}{\Gamma_g}. \tag{13}$$

To better understand η_s, consider the plane strain case that corresponds to Fig. 1, and assume that all surface steps are straight and parallel to the grain boundaries. If η_s is uniform over the surface of the grain, then it will be equal to λ divided by the average number of steps that are on the surface of one grain. However, η_s is actually the local value at the grain boundary, and certain phenomena can cause η_s to differ from the average value for the entire grain surface. An example of this is a grain boundary groove, where steps are closer together such that η_s is smaller than the average value for the grain. On an atomic scale, η_s will also vary as steps move towards the grain boundary during growth. However, η_s in Eq. (13) can still be approximated as a constant, if it is a time-averaged quantity (this is discussed further in Sec. IV). On a surface that is extremely rough on an atomic scale, η_s might approach 1. At the other extreme, $\eta_s>\lambda$ corresponds to a step density less than 1 per grain, which can occur if step creation is particularly difficult. This suggests that there is no upper limit on η_s, although a particularly large value would result in extremely slow growth. In general, Γ_c/Γ_g should be significantly less than 1, since attaching an adatom at a surface growth site is easier than inserting an adatom into the surface layer (even at the grain boundary). Thus, based on the physics associated with η_s and Γ_c/Γ_g, it appears that ω_c can take on a wide range of values,

While wmc effects are potentially interesting, it is first instructive to consider conditions where wmc variations can be ignored. This occurs in films that are thick enough to make the γ_s wmc contribution negligible. In this case, evaluating the integral in Eq. (11) leads to

$$\Delta\epsilon=\frac{1}{\beta}\ln\left[1+(\exp[\beta\Delta\epsilon_0]-1)\exp\left(-\frac{2\beta\omega_c}{\lambda}\Delta n\right)\right], \tag{14}$$

where $\Delta\epsilon=\epsilon-\epsilon_{ss}$ and $\Delta\epsilon_o=\epsilon_o-\epsilon_{ss}$. Replacing s_s with $\exp(-\beta\epsilon_{ss})$ according to Eq. (12) is convenient here, since ϵ_{ss} can be obtained directly from experiments. Using Eq. (14), four examples of $\Delta\epsilon$ vs Δn profiles are plotted in Fig. 2. In Fig. 2(a), ϵ_{ss} is reached almost instantaneously (i.e., within several atomic layers), and the strain gradient is essentially nonexistent. In Fig. 2(b), a strain gradient evolves over part of the film thickness, followed by a constant steady-state strain of ϵ_{ss} for the remainder of the film thickness. In Fig. 2(c), a strain profile exists over the entire film thickness. The fourth case in Fig. 2(d) corresponds to a negligible compressive stress, due to a very low value of ω_c (i.e., atom insertion occurs very slowly).

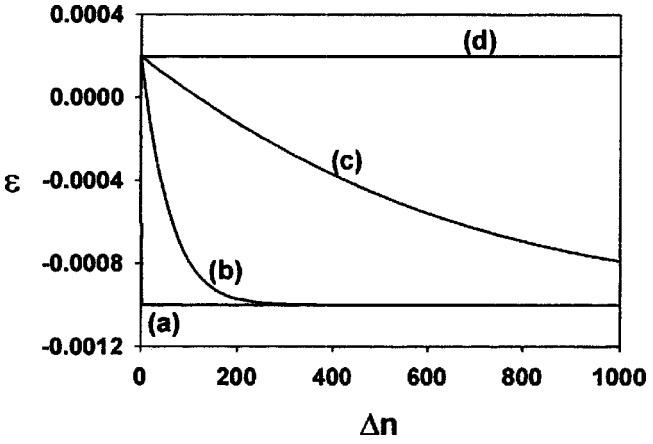

FIG. 2. Strain (ϵ) vs change in film thickness (Δn), based on Eq. (14), for $\beta=500$, $\lambda=500$, $\epsilon_o=0.0002$, and $\epsilon_{ss}=-0.001$; and (a) $\omega_c=1$, (b) $\omega_c=0.01$, (c) $\omega_c=0.001$, and (d) $\omega_c=10^{-7}$.

The three cases in Figs. 2(a)–2(c) can be distinguished from one another by considering the film thickness where the strain reaches its steady-state value. Rigorously, this occurs as Δn approaches infinity. However, the strain attains most of its steady state value at $\Delta\epsilon=0.01\Delta\epsilon_o$, which leads to

$$\Delta n_{ss}=\frac{\lambda}{2\beta\omega_c}\ln\left[\frac{\exp(\beta\Delta\epsilon_o)-1}{\exp(0.01\beta\Delta\epsilon_o)-1}\right]. \tag{15}$$

Values of Δn_{ss} according to Eq. (15) are plotted in Fig. 3, as a function of the kinetic ratio ω_c. For a given value of ω_c, strain gradients occur when the film thickness is less than Δn_{ss}. The behavior in Fig. 2(a), where the strain reaches ϵ_{ss} in several atom layers or less, only occurs when ω_c is relatively large. The difference between Fig. 2(b) where the strain reaches steady state and Fig. 2(c) where gradients exist across the entire film thickness is determined by whether or not the film thickness exceeds the steady-state value, Δn_{ss}.

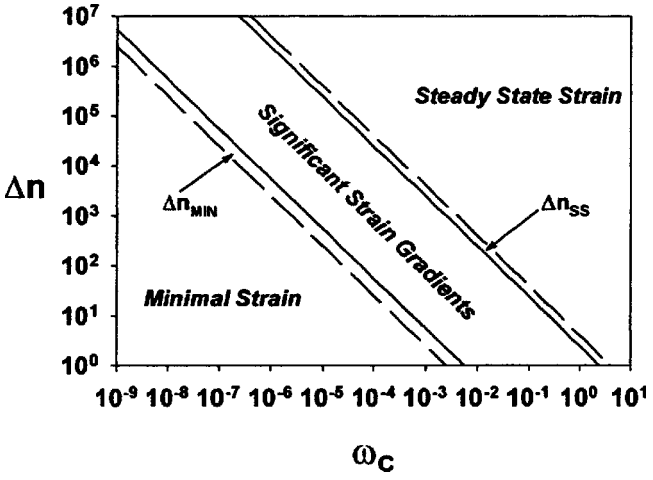

FIG. 3. Δn_{MIN} according to Eq. (14) with $\Delta\epsilon=10^{-5}$ and Δn_{SS} according to Eq. (15). All calculations were performed with $\beta=500$, $\lambda=500$, and $\epsilon_o=0.0002$. The solid and dashed lines correspond to $\epsilon_{ss}=-0.001$ and $\epsilon_{ss}=-0.01$, respectively.

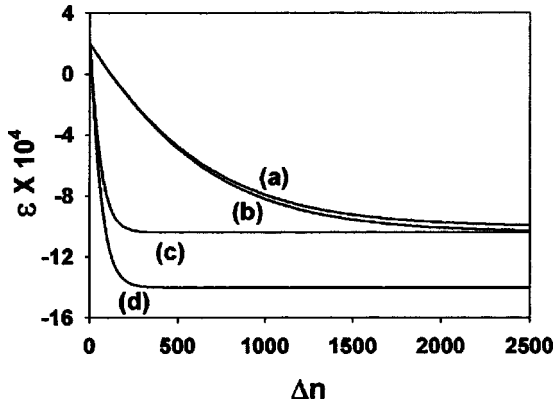

FIG. 4. Strain (ϵ) vs change in film thickness (Δn) with $\beta=500$, $\omega_c=0.001$, $\ln s_s^o=0.5$, $\epsilon_o=0.0002$, and $\psi_s/n_o\sim 0$: (a) $\psi_b=1$, $\lambda=500$, (b) $\psi_b=10$, $\lambda=500$, (c) $\psi_b=1$, $\lambda=50$, and (d) $\psi_b=10$, $\lambda=50$.

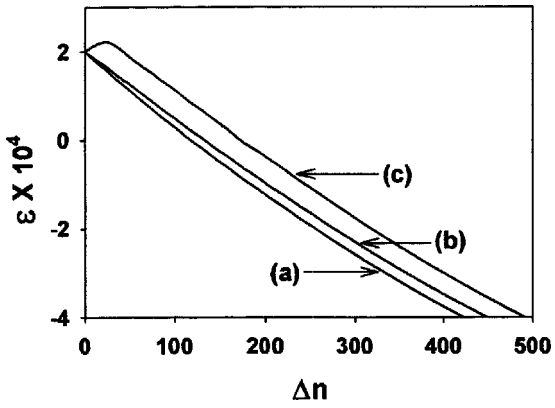

FIG. 5. Strain (ϵ) vs change in film thickness (Δn) with $\beta=500$, $\omega_c=0.001$, $\ln s_s^o=0.5$, $\epsilon_o=0.0002$, and $\psi_b=\psi_s=10$: (a) $n_o=500$, (b) $n_o=50$, and (c) $n_o=5$.

The case of negligible compressive stress [e.g., Fig. 2(d)] is defined here as a film where $\Delta\epsilon<10^{-5}$. This condition was used with Eq. (14) to calculate the values of Δn_{MIN} that define the lower boundaries in Fig. 3. Thus, significant strain gradients occur in the middle region of Fig. 3. Steady-state strain is reached above and to the right of this region, and negligible strain occurs below and to the left of this region.

Variations in ϵ_{ss} and ϵ_o have only a moderate effect on Fig. 3. For example, the dashed lines correspond to a significantly larger value of $\epsilon_{\mathrm{ss}}=-0.01$ (i.e., an increase in s_S of almost two orders of magnitude). This produces only a modest change in the diagram. Thus, for a film with a given grain size, the kinetic ratio ω_c is the dominant factor that determines the strain profile.

B. Grain size, film thickness, and weighted-mean curvature

Variations in the grain dimensions L and H (i.e., λ and n) can affect strain evolution in several ways. It is first instructive to compare the magnitudes of the two wmc contributions by setting the time derivative in Eq. (10) to zero to obtain:

$$\hat{\epsilon}_{\mathrm{ad}}=-\frac{\ln s_s^o}{\beta}-\frac{\psi_b}{\beta\lambda}+\frac{\psi_s}{\beta n}=\epsilon_{\mathrm{ss}}+\frac{\psi_s}{\beta n}. \tag{16}$$

This quantity is the strain that is in equilibrium with C_a, accounting for both the supersaturation associated with the growth flux (s_s^o) and the wmc contributions. For the geometry in Fig. 1, the ψ_b wmc contribution is constant, but the ψ_s wmc contribution causes $\hat{\epsilon}_{\mathrm{ad}}$ to vary as the film grows, approaching ϵ_{ss} asymptotically as n increases enough to make the last term negligible.

Several different comparisons are used to illustrate the relationships between grain size and stress evolution in Figs. 4–6. All of these examples show ϵ vs Δn, which are strain profiles that evolve from the initial condition $\epsilon=\epsilon_o$ at $n=n_o$. Cases where ψ_s wmc effects are negligible are first considered in Fig. 4, based on Eq. (14). In this expression, the grain size λ affects stress evolution through the second exponential term and ϵ_{ss} depends on ψ_b/λ [via Eqs. (9) and (12)]. Both of these influences are evident in the strain profiles plotted in Fig. 4. As seen in Eq. (16), the magnitude of ψ_b/λ, determines whether this contribution will be significant. The value of ψ_b is typically between 1 and 10 (e.g., $a=0.2$ nm, $T=1000$ K, and $\gamma_s=0.35$ J/m^2 give $\psi_b=1$, $T=290$ K, and $\gamma_s=1.0$ J/m^2 give $\psi_b=10$). In Fig. 4(a) the ψ_b wmc effect is small, such that the strain profile is almost identical to Fig. 2(c) [i.e., the steady-state strain is only shifted by $\psi_b/\beta\lambda=4(10)^{-6}$, as indicated by Eq. (16)]. With $\lambda=500$, increasing ψ_b from 1 to 10 produces only a small shift from profile (a) to profile (b) (i.e., the wmc contribution is still relatively small). Decreasing the grain size to $\lambda=50$ has two primary consequences. First, the increase from $\psi_b=1$ to $\psi_b=10$ leads to a more substantial wmc contribution which in turn produces a significant difference between the steady-state strains in profiles (c) and (d) [note that profiles (b) and (c) evolve to the same steady-state strain value because the magnitude of the ψ_b wmc contributions are identical]. The other effect of decreasing λ to 50 is that profiles (c) and (d) both reach steady state at a much faster rate because of the λ dependent exponential term in Eq. (14). Physically, this occurs because a film with smaller grains has proportionally more grain boundary sites for atom insertion.

To examine how the ψ_s wmc term affects strain evolution, Eq. (11) was integrated numerically to obtain Figs. 5 and 6. These results depend on the absolute film thickness n, in contrast to those in Fig. 4, which depend only on Δn. In

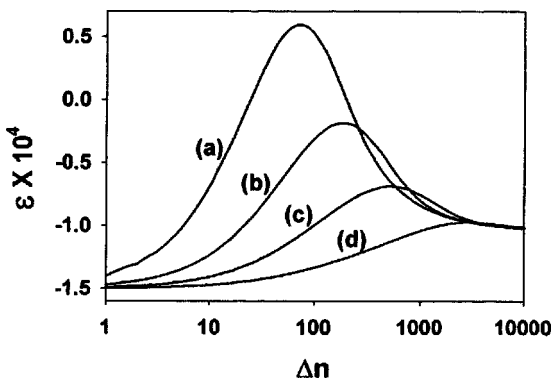

FIG. 6. Strain (ϵ) vs change in film thickness (Δn) with $\beta=500$, $\lambda=500$, $\psi_b=1$, $\psi_s=10$, $n_o=50$, $\ln s_s^o=0.05$, and $\epsilon_o=-0.00015$: (a) $\omega_c=0.01$, (b) $\omega_c=0.003$, (c) $\omega_c=0.001$, and (d) $\omega_c=0.0003$.

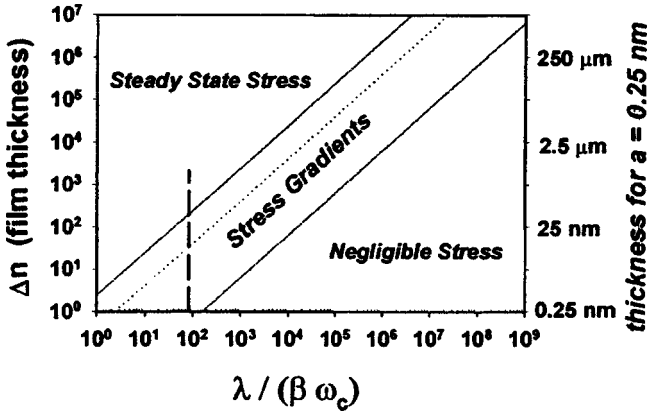

FIG. 7. Stress evolution regimes as a function of the length scales λ and Δn, with $\epsilon_o = 0.0$, $\ln s_s^o = 0.5$, and $\psi_b = \psi_s = 0$. The dotted line shows the thickness where the film strain reaches 50% of ϵ_{ss}.

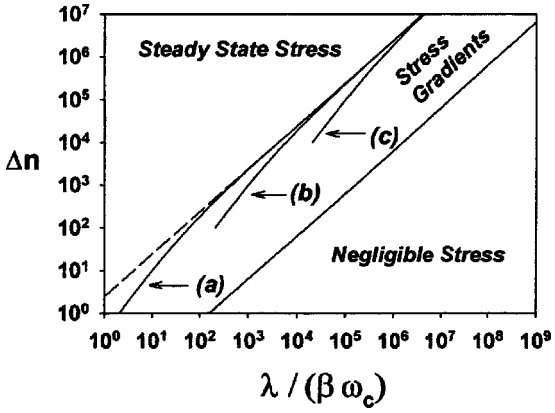

FIG. 8. Stress evolution regimes with $\ln s_s^o = 0.5$, $\epsilon_o = 0.0$, and $\psi/n_o = 0$: (a) $c = 1$, (b) $c = 100$, (c) $c = 10\,000$ (where $c = \psi_b/\beta\omega_c$, as noted in the text). The dashed line shows the comparable $\psi_b = 0$ result from Fig. 7 for comparison (relative to Fig. 7, changes in the lower boundary are too small to be noticeable in this diagram).

Fig. 5, the effect of varying n_o is examined for cases where the steady state is relatively large. Even with a relatively large value of $\psi_s = 10$, profile Fig. 5(a) is almost identical to Figs. 4(a) and 4(b), where contributions associated with ψ_s were ignored. Decreasing n_o produces relatively small changes in this profile, although in Fig. 5(c), ψ_s/n_o is large enough to cause an initial strain increment in the tensile direction. Physically, this occurs because the aspect ratio of the grains (relatively small H and large L) creates a driving force to move material out of the grain boundary. This effect is more pronounced for the examples in Fig. 6, where variations in ω_c are considered for cases where the steady-state strain is relatively small. These profiles were obtained for a relatively large value of $\psi_s = 10$ and a more moderate value of $\psi_b = 1$, a difference that promotes initial tensile stress. To see this, note that tensile strain requires a positive value of $\hat{\epsilon}_{ad}$ in Eq. (16). Rearranging this expression shows that tensile values occur when the grain aspect ratio, n/λ, is less than $(\psi_s - n \ln s_s^o)/\psi_b$. In general, the wmc effects associated with ψ_s are only significant with relatively small stresses. This is evident in comparing Fig. 5 with the more prominent tensile behavior in Fig. 6. For a material with $M = 200$ GPa, the two supersaturation levels in Figs. 5 and 6 (i.e., $\ln s_s^o$ of 0.5 and 0.05) correspond to steady-state stresses of -200 and -20 MPa, respectively.

Figures 7–9 use boundaries similar to those in Fig. 3, to show the general behavior of strain profiles as a function of the two key length scales, λ and Δn. In these diagrams the value of λ is normalized by $\beta\psi_c$ [from Eqs. (11) and (13), recall that β reflects elastic and thermal energies, and ω_c is a kinetic ratio of the atom insertion and growth rates]. This scaling makes it possible to represent a wider range of possibilities in a single figure. With the geometry in Fig. 1, a particular material and a specific set of growth conditions correspond to a fixed value of $\lambda/\beta\omega_c$. The boundaries in Fig. 7 are based on the limiting case where the wmc contributions are negligible (i.e., $\psi_b \sim 0$ and $\psi_s \sim 0$). As the film grows beyond the coalescence point, Δn increases and the growth process corresponds to a vertical line if the grain size, λ, is fixed. Significant strain develops by the time Δn reaches the lower boundary, and the strain is essentially at steady-state when Δn reaches the upper boundary. An example of this is shown by the dashed vertical line, which is based on the AlN film in Sec. III C. It is also possible to use this type of diagram to obtain insight into films where the grain size increases as deposition proceeds. For example, with a columnar microstructure where the grain size increases gradually during film growth, the vertical line would be replaced by a line with a positive slope. The dotted line in Fig. 7 shows the film thickness where the strain reaches 50% of its steady-state value. Contours for other strain levels can also be added, so that this type of diagram can incorporate additional quantitative information about strain profiles.

Figure 7 provides a convenient representation of the film thickness regimes where negligible stress, significant gradients, and steady-state stress will occur. Figures 8 and 9 illustrate how the wmc contributions can alter this representation. First, consider films that are thick enough to neglect ψ_s (as already discussed in conjunction with Fig. 4). The remaining wmc contribution associated with ψ_b then causes only modest changes in going from Fig. 7 to 8. Cases (a), (b), and (c) in Fig. 8 show the effect of varying the grain size λ, with all

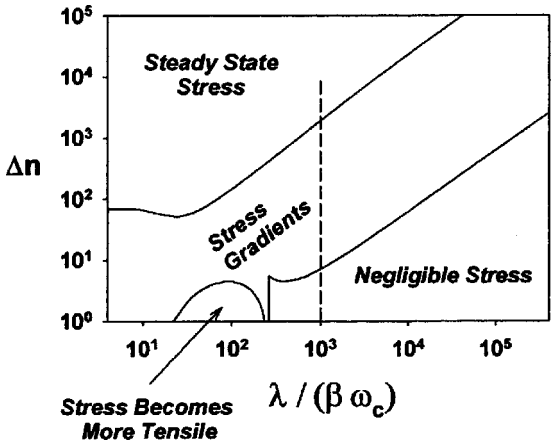

FIG. 9. Stress evolution regimes with $\ln s_s^o = 0.5$, $\epsilon_o = 0.0002\ (500/\lambda)^{1/2}$, $n_o = \lambda/10$, $\beta = 500$, $\omega_c = 0.001$, and $\psi_b = \psi_s = 10$. The dashed, vertical line corresponds to the conditions in Fig. 5(b).

other parameters fixed. For each of these, the lumped constant $c=\psi_b/\beta\omega_c$ was assigned a fixed value (which is somewhat more general than assigning values for each of these quantities separately). Now recall that Eq. (14) contains two terms that depend on the grain size, $\lambda/\beta\omega_c$ and ψ_b/λ. Thus, increasing $\lambda/\beta\omega_c$ along the horizontal axis by varying only λ, means that ψ_b/λ must undergo a corresponding decrease. The given, fixed value of c imposes an effective lower limit as follows: $(\lambda/\beta\omega_c)^{\mathrm{LB}}=\lambda^{\mathrm{LB}}/(\beta\omega_c)^{\mathrm{UB}}=(\lambda^{\mathrm{LB}}/\psi_b^{\mathrm{UB}})c$. Here, the superscripts LB and UB refer to lower and upper bounds. The minimum practical value of λ^{LB} is taken to be $\sim$10. (A slightly lower value might be reasonable for extremely small grains, but λ^{LB} must be greater than 1.) As noted above, an approximate value of $\psi_b^{\mathrm{UB}}\sim 10$ is reasonable for many materials. This leads to $(\lambda/\beta\omega_c)^{\mathrm{LB}}\sim c$. Thus, boundaries (a), (b), and (c) in Fig. 8 are terminated according to this limit, with the understanding that this cutoff is approximate. These wmc effects on the upper boundary in Fig. 8 are more pronounced for smaller grain sizes. The lower boundary for $\Delta\epsilon=10^{-5}$ also shifts, but this change is so small that it cannot be discerned in Fig. 8.

Including ψ_s wmc contributions leads to more complex diagrams that are more sensitive to changes in certain parameters (i.e., other than $\lambda/\beta\omega_c$). An example of this is shown in Fig. 9. Here, the initial aspect ratio, λ/n_o, is constant. Note that this ratio varies for the plots in Fig. 5 and is fixed for the plots in Fig. 6 (it is not relevant for Figs. 4, 7, and 8). For Fig. 9, a fixed initial aspect ratio provides a better basis for comparison than a fixed initial film thickness, primarily because the film thickness at coalescence increases as the grain size increases. To understand this, consider the growth of isolated grains prior to impingement. With a periodic array of grains, λ is equivalent to the initial island spacing. The film thickness at impingement is then determined by the relative growth rates of the two facets (e.g., a value of $\lambda/n_o=10$ indicates that the lateral growth rate of each of the two side facets is five times faster than the normal growth rate of the top facet). Thus, for a given set of deposition conditions, one expects fixed facet growth rates, and hence, a fixed value of λ/n_o. In this case, different values on the horizontal axis in Fig. 9 correspond to different grain sizes for a fixed set of growth conditions (i.e., $\beta\omega_c$ is also fixed).

To construct self-consistent diagrams in Fig. 9, ϵ_o variations as a function of grain size are incorporated into the analysis. In Sec. I, it was noted that the initial, intrinsic strain, ϵ_o has been associated with at least two different phenomena: compressive strain due to the Laplace pressure in isolated islands and tensile strain due to grain boundary formation during island coalescence. To illustrate these possibilities, the examples in Figs. 4–6 were created with both tensile and compressive values for ϵ_o. In recent years, several relationships of the form $\epsilon_o=A\lambda^B$ have been proposed for intrinsic tensile strains, where A and B are constants determined by the mechanistic details.[7,11,18] In Fig. 9, the following relationship was used: $\epsilon_o=0.0002(50/\lambda)^{1/2}$. The exponent here corresponds to the Nix and Clemens analysis,[11] and the other values were chosen to be consistent with the profile in Fig. 5(b) [i.e., so that the dashed line in Fig. 9 corresponds exactly to the profile in Fig. 5(b)].

In comparing Figs. 7 and 9, there are several differences. First, the steady-state strain boundary is shifted at smaller grain sizes. This is caused by wmc contributions that are more substantial at smaller length scales, as described earlier. A second difference is the small region in the lower left of Fig. 9 where stress initially moves in the tensile direction, similar to Figs. 5(c) and 6. The boundary that defines this region is the maximum in the ϵ vs Δn profiles. This is found by taking the derivative of Eq. (11), setting $d\epsilon/d(\Delta n)=0$, and rearranging to give

$$\Delta n^*=-n_0+\frac{\psi_s}{\dfrac{\psi_b}{\lambda}+\beta(\epsilon^*-\epsilon_{\mathrm{ss}}^o)}, \tag{17}$$

where Δn^* and ϵ^* are the film thickness and strain values at the maximum. In this expression, ϵ^* must be determined with Eq. (11), so the Δn^* values in Fig. 9 were obtained by evaluating Eqs. (11) and (17) numerically. A stress profile that begins in the tensile region of Fig. 9 will reach a maximum tensile value at a film thickness of Δn^*. After this, the stress will move in the compressive direction, and then eventually reach a steady-state compressive value if and when Δn exceeds Δn_{ss}(Δn_{ss} is discussed in connection with Fig. 3).

In Fig. 9, the lower boundary associated with negligible stress is terminated at $\lambda/\beta\omega_c=258.3$. This corresponds to the largest grain size where an initial rise in tensile stress can occur [i.e., this value was obtained by solving Eq. (17) for $\Delta n^*=0$ and $\epsilon^*=\epsilon_o$]. At grain sizes larger than this limiting value, the negligible strain boundary in Fig. 9 is similar to Fig. 7. Below this limit, the stress increment initially occurs in the tensile direction, such that a compressive shift of $\Delta\epsilon=10^{-5}$ does not necessarily imply minimal strain. Thus, the negligible strain boundary in Fig. 9 terminates at $\lambda/\beta\omega_c=258.3$.

In summary, Fig. 7 is convenient because it represents strain profiles for a variety of different films where grain boundary diffusion and wmc effects are negligible. The effects of ψ_b wmc contributions are incorporated into Fig. 8, such that boundaries (a), (b), and (c) correspond to fixed values of β, ω_c, and ψ_b, where only λ varies. The ψ_b wmc contributions lead to some loss in generality, because the ratio $\lambda/\beta\psi_c$ can no longer strictly be used to consider independent variations in λ, β, or ω_c. The diagram in Fig. 9 accounts for both types of wmc contributions, and is less general than Fig. 8. Here, the boundaries undergo more significant variations for different values of ϵ_o, s_s^o, and other parameters (particularly in films where effects associated with ψ_s are more pronounced because of relatively low strains and relatively large values of ψ_s/n). Thus, the diagram in Fig. 9 is no different from a plot of Δn vs λ, although the $\lambda/\beta\omega_c$ scaling is still used here to facilitate direct comparison with Fig. 7. In Fig. 9 the observation that ϵ_o and s_s^o can have a significant influence on strain evolution differs from the conclusion that was drawn from Fig. 3. This occurs primarily because of the combined effects of smaller strains and relatively large values of $(\psi_s\lambda/\psi_b n)$.

C. Comparison with experiments

Most of the data in the literature do not permit direct comparisons with the calculated results in Secs. III A and III B. One impediment is that intrinsic stresses in most films are produced by more than one mechanism. The mechanism described in Sec. II is best studied under conditions where only compressive stress is observed and where grain boundary diffusion is negligible. These requirements can be met approximately during the later stages of AlN growth by molecular beam epitaxy (MBE), where compressive stress is dominant after roughly 2 h of growth.[6] The stress in these films does not change during postdeposition annealing, which suggests that grain boundary diffusion is negligible. This differs from many metal films where annealing relieves stress when grain boundary diffusion is fast enough to move atoms out of a compressively strained film, to the external surface (e.g., Ag films[5,15]).

Stress profiles in AlN were obtained from *in situ* curvature measurements. The data in Fig. 10(a) show average stresses obtained from the standard Stoney's equation analysis of curvature data.[6,19] With fixed grain size and negligible grain boundary diffusion, the slope of the data in Fig. 10(a) were converted to the stress profile, part of which is shown in Fig. 10(b).[6] In comparison to the average film stresses in Fig. 10(a), the stresses in Fig. 10(b) correspond to the incremental material that is added during growth at a particular point in time. Thus, Fig. 10(b) shows the strain gradient in this portion of the film. To fit Eq. (14) to the results in Fig. 10(b), values of n_o and ϵ_o must be inferred from the data. In the derivation in Sec. III, this initial condition corresponds to the point where all of the islands simultaneously impinge on one another to create a continuous film. The real islands do not have a uniform spacing and size, so coalescence occurs more gradually. The data can still be analyzed with Eq. (14) by recognizing that the initial condition $\epsilon=\epsilon_o$ at n_o can be invoked for any value of n after the film has completely coalesced. Since the experiments show an initial regime where tensile stress dominates, only data where the instantaneous stress is compressive were considered. This corresponds to setting ϵ_o to zero, which occurs at roughly $n_o=690$. The eventual steady-state value of $\epsilon_{ss}=-0.17$ was also obtained from the experimental results in Fig. 10(b). Note that the data show a nearly constant value for ϵ_{ss}, which implies that wmc variations with increasing n are small enough to be ignored here. With these values of ϵ_o, n_o, and ϵ_{ss}, fitting the model then gives a value of the only unknown lumped quantity in Eq. (11), $\beta\omega_c/\lambda=0.0123$. Values of $\beta=551$ and $\lambda=259$ obtained from the experimental conditions and known physical constants then lead to $\omega_c=0.0058$. The predicted stress profile associated with this fit is shown as the solid line in Fig. 10(b), and is also plotted in Fig. 7. Moderate variations in the choice of ϵ_o and n_o produce relatively small changes in the ω_c value obtained from this fit. With larger variations in ϵ_o and n_o, fitting the data to Eq. (14) is not appropriate [i.e., at smaller n_o Eq. (14) does not properly account for the tensile portion of the stress profile, and at larger values of n_o the initial strain is too close to the steady-state value].

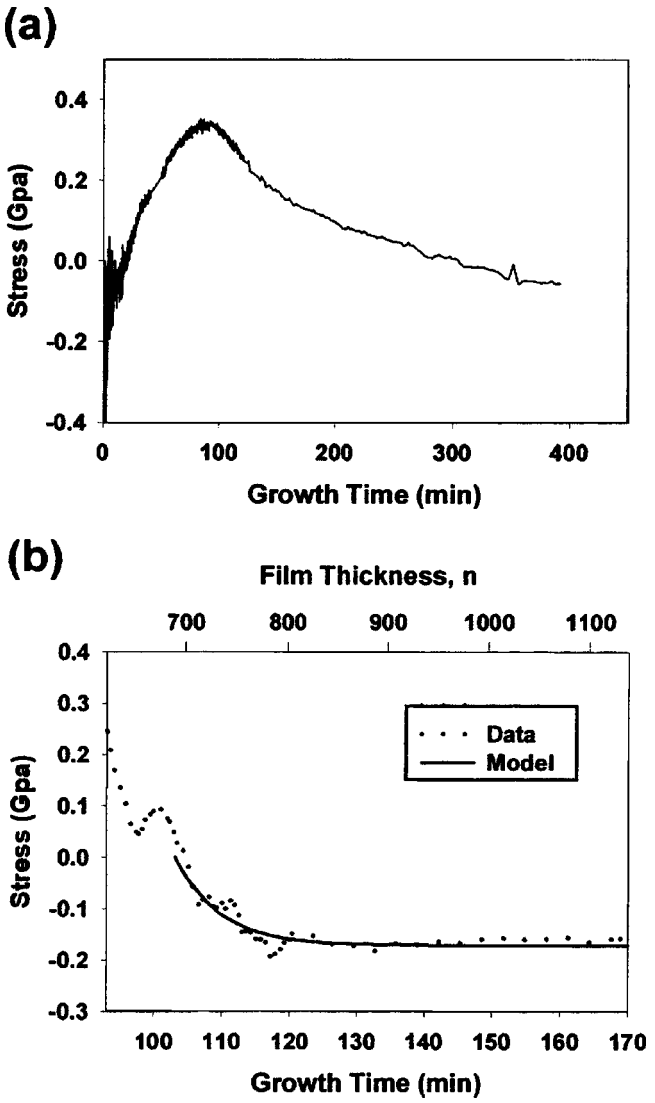

FIG. 10. Growth stress in MBE grown AlN, determined by *in situ* curvature measurements. Films were deposited on (111) Si, at 700 °C. Additional experimental details are reported in Ref. 7. (a) Average film stress vs time, based on Stoney's equation; (b) stress profile obtained from the slope of the data in Fig. 10(a) (Ref. 7). The top axis in Fig. 10(b) is n, based on the growth time, the measured growth rate of 100 nm/h, and $a=0.249$ nm (0002 spacing for AlN).

The fit in Fig. 10(b) demonstrates the basic procedure that can be used to analyze experimental results with the model obtained in Sec. II. One potential problem with this example is that the tensile stress mechanism may still have some influence even after the incremental stress becomes compressive. Assessing the competition between the tensile and compressive mechanisms is beyond the scope of this article, however, a significant contribution from this mechanism would imply a value of ω_c that is somewhat larger than 0.0058. Additional experiments with AlN will allow us to deconvolute these effects. The type of data required to more fully test the model in section II is currently not available for any system.

IV. DISCUSSION

As noted in Sec. I, significant compressive stresses are often associated with high surface mobilities. However, the

surface mobility is not considered directly in Sec. II, thus its relationship to the intrinsic stress is not immediately apparent. Based on Eqs. (9) and (12), the steady-state strain for a material where wmc effects are small and the grain size is fixed depends only on the thermodynamic driving force $\delta\mu_G$ (the excess chemical potential of surface adatoms due to the growth flux). As noted in Sec. II B, $\delta\mu_G$ is perhaps best conceptualized in terms of the adatom concentration on the surface, C, where $C=C^o$ corresponds to $\delta\mu_G=0$. To see possible relationships between the surface mobility and $\delta\mu_G$ or C, one must go beyond the thermodynamic treatment in Sec. II and consider the interrelated effects of various kinetic mechanisms, including adsorption, surface diffusion, and the nucleation of two-dimensional islands on the growth surface. These processes have been studied extensively.[20] For present purposes, we are interested in a simple discussion of the relationships between surface processes and the value of C_a.

Recall that the insertion mechanism responsible for compressive stress is related to C_a, which is the value of C in the vicinity of the grain boundary [see Eq. (5)]. A relatively simple example is described here to show how C_a can be affected by surface diffusion. The schematics in Fig. 11 depict the motion of atomic steps near the grain boundary. During growth the terrace width adjacent to the grain boundary varies because of step motion, such that η_s in Eq. (13) is an average terrace width, as already noted. This temporal averaging also applies to the value of C_a. To illustrate this, consider the simplest case where η_s is relatively independent of $\delta\mu_G$ (an oversimplification), and the atom insertion rate into the grain boundary is always slow relative to the surface mobility. This leads to the schematic C_a profiles in Fig. 11, which are dictated by the kinetic tradeoff between surface diffusion and the rate at which adatoms are attached to the moving step. The limiting case of fast surface diffusion corresponds to the flat adatom concentration in Fig. 11(a), whereas Figs. 11(b) and 11(c) show profiles with a surface diffusivity that is slow enough to create a depletion zone in the vicinity of the growing step. Since the steps move towards the grain boundary during film growth, the terrace width adjacent to the grain boundary decreases as the step moves (until the step reaches the boundary, where η_s will then be determined by the subsequent layer). With the slower surface mobility scenario in Figs. 11(b) and 11(c), the value of C_a decreases when the terrace width is smaller than the depletion zone. This is shown schematically here as $C_a^{(c)} < C_a^{(b)}$. Thus, Figs. 11(b) and 11(c) provide a conceptual description of how C_a can decrease as the step moves towards the grain boundary. Based on this behavior, C_a is best understood as an average value over the relatively short temporal fluctuations associated with step motion (similar to η_s). Since the value of C_a is represented by the value of s_s (and hence ϵ_{ss}) in many of the expressions in Secs. II and III, it follows that s_s should also be understood as an average value. Therefore, based on the possible fluctuations of C_a depicted in Fig. 11, a lower surface mobility can decrease the value of s_s and thus decrease ϵ_{ss} in accordance with Eq. (12). As noted above, a more realistic description must include other surface processes in addition to those in Fig. 11. For example, higher supersaturations will increase the nucleation

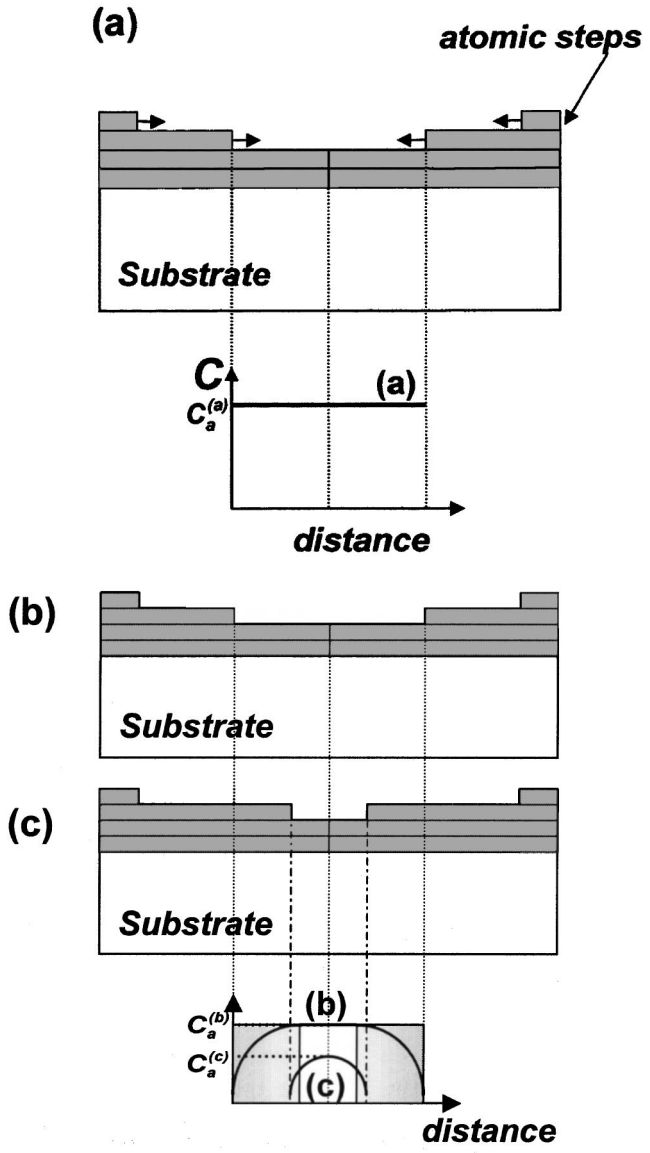

FIG. 11. Schematice showing hypothetical adatom concentrations along the growth surface. (a) Surface diffusion is fast, such that C is uniform. (b) Slower surface diffusion creates a depletion zone near the growth steps. In the C vs distance profile for this case, the depletion zone is shaded. (c) Similar to (b), except that additional growth has caused the lowest step to move towards the grain boundary. In this case, the entire profile falls in the depletion zone [the depletion zone is not shaded here, to avoid confusion with profile (b)]. For the three different profiles shown here, the adatom concentrations at the grain boundaries are labeled as $C_a^{(a)}$, $C_a^{(b)}$, and $C_a^{(c)}$.

of two-dimensional clusters on the growth surface and increase the density of surface steps. A detailed treatment of these processes is beyond our current scope, however, higher surface mobilities should correspond to higher s_s for many cases.

In addition to affecting the steady-state strain, the surface mobility can also influence the strain evolution kinetics. As described in Sec. III, the kinetics are primarily described by ω_c, however, the surface mobility does not appear explicitly in ω_c. With ω_c given by Eq. (13), note that η_s depends on a variety of surface-related kinetic mechanisms, as discussed in the previous paragraph. This suggests that η_s, and hence ω_c, will vary with changes in the surface diffusivity.

The jump frequencies that appear in Eq. (13), Γ_c and Γ_g, are distinctly different than the jump frequency associated with surface migration. While one might expect a material with high surface mobilities to also exhibit relatively high values of Γ_c and Γ_g (at least in some cases), the ratio Γ_c/Γ_g that appears in the expression for ω_c [Eq. (13)] will not necessarily scale with the surface mobility.

The thermodynamic and kinetic considerations discussed above indicate that s_s and ω_c can be affected by the surface mobility, even though these relationships are not given explicitly in the model formulation. There are several other factors that are not incorporated into the current model. In particular, note that grain size effects only enter the current model through the wmc contributions and in one term of the governing rate expression [Eq. (10)]. Surface roughness and grain boundary grooving will introduce additional length scale issues that should be incorporated into a more detailed model. For example, surface roughness effects will create more complex strain distributions.[7,18,21] Grain boundary grooving can contribute to these roughness effects, although, if the grooves are small compared to L, then they will only cause small deviations from the geometry in Fig. 1. Local effects such as the strain fields associated with grain boundary dislocations are also ignored here (i.e., they are averaged over the length of the boundary), and variations in γ_b due to the insertion of excess atoms are also ignored for simplicity.

The initial tensile stress mechanism observed in AlN (and in many other systems) will modify Fig. 7, as will grain size distributions, the evolution of columnar microstructures, and some of the other effects noted in the preceding paragraph. To elucidate these effects, more detailed experiments are required. Grain size effects (i.e., changes in λ) are perhaps the most obvious feature that should be subjected to experimental tests. Experimentally derived versions of the diagrams in Figs. 7–9 would provide important insight into possible deviations from the model predictions. The wmc effects in Figs. 8 and 9 are relatively subtle, and will thus be more difficult to verify. In films where the steady-state strains are sufficiently small, it may be possible to detect wmc effects associated with relative tensile strains if the film thickness at coalescence is small enough. However, this will require careful experiments and analysis. *A priori* information about the surface and interfacial energies from either experiments or atomistic calculations will also facilitate investigations into wmc effects.

V. CONCLUSIONS

The model developed in Secs. II and III considers compressive stress evolution in the absence of grain boundary diffusion. This description provides some relatively basic insights into the proposed mechanism. First, we propose a model where the surface supersaturation, s_s, is the key thermodynamic factor that determines the steady-state compressive strain. The kinetics associated with stress evolution are also described by a single parameter, ω_c (i.e., for a film with a given values of λ and β). In the absence of wmc effects, four types of stress profiles were categorized in Figs. 2 and 3. A somewhat more general diagram showing the regimes in Fig. 3 was also presented in Fig. 7, in terms of the two key length scales λ and n. This thinking was also extended to include wmc effects. Although these are often negligible, they can become noticeable with larger surface and interface free energies, and at smaller grain sizes and film thickness. Perhaps the most interesting wmc effect is the possibility that the initial stress can move in the tensile direction, although this only occurs under a limited range of conditions.

The types of diagrams in Figs. 7–9 provide relatively general descriptions of postcoalescence growth stress in polycrystalline films. Detailed experiments on different systems are needed to verify and refine these calculated results. A key reason that real films are likely to deviate from these model predictions is that real microstructures will differ considerably from the model geometry in Fig. 1 (this picture is probably most appropriate for columnar microstructures where L is relatively constant). Also, the model developed here describes only intrinsic compressive stresses created by inserting excess atoms at grain boundaries. To accurately describe the complete stress profile in most materials, this must be combined with models for other mechanisms. Future model development will also incorporate grain boundary diffusion and more detailed descriptions of kinetic processes at the growth surface.

ACKNOWLEDGMENTS

Primary research support from the National Science Foundation, under Award No. DMR-0305418, is gratefully acknowledged. Additional support from NSF-DMR-0079964 and DOE-DE-FG02-95ER25239 is also acknowledged. Mike Aziz, Harvard University, is acknowledged for suggesting the possible role of weighted mean curvature.

[1] R. Abermann and R. Koch, Thin Solid Films **129**, 71 (1985).
[2] R. Koch J. Phys.: Condens. Matter **6**, 9519 (1994).
[3] A. L. Shull and F. Spaepen, J. Appl. Phys. **80**, 6243 (1996).
[4] J. Proost and F. Spaepen, J. Appl. Phys. **91**, 204 (2002).
[5] J. Floro, S. J. Hearne, J. A. Hunter, P. Kotula, E. Chason, S. C. Seel, and C. V. Thompson, J. Appl. Phys. **89**, 4886 (2001).
[6] A. Rajamani, R. Beresford, and B. W. Sheldon, Appl. Phys. Lett. **79**, 3776 (2001).
[7] B. W. Sheldon, K. H. A. Lau, and A. Rajamani, J. Appl. Phys. **90**, 5097 (2001).
[8] R. C. Cammarata, T. M. Trimble, and D. J. Srolovitz, J. Mater. Res. **15**, 2468 (2000).
[9] R. W. Hoffman, Phys. Thin Films **3**, 211 (1966).
[10] F. A. Doljack and R. W. Hoffman, Thin Solid Films **12**, 71 (1972).
[11] W. D. Nix and B. M. Clemens, J. Mater. Res. **14**, 3467 (1999).
[12] A. Rajamani, B. W. Sheldon, E. Chason, and A. F. Bower, Appl. Phys. Lett. **81**, 1204 (2002).
[13] M. F. Doerner and W. D. Nix, CRC Crit. Rev. Solid State Mater. Sci. **14**, 225 (1988).
[14] R. Abermann, Vacuum **41**, 1279 (1990).
[15] E. Chason, B. W. Sheldon, L. B. Freund, J. A. Floro, and S. J. Hearne, Phys. Rev. Lett. **88**, 156103 (2002).
[16] V. Ramaswamy, Ph.D. thesis, Stanford University, 2000.
[17] J. E. Taylor, Acta Metall. Mater. **40**, 1475 (1992).
[18] L. B. Freund and E. Chason, J. Appl. Phys. **89**, 4866 (2001).
[19] G. G. Stoney, Proc. R. Soc. London **82**, 172 (1909).
[20] J. A. Venables, *Introduction to Surface and Thin Film Processes* (Cambridge University Press, Cambridge, U.K., 2000).
[21] H. T. Johnson and L. B. Freund, J. Appl. Phys. **81**, 6081 (1997).